SANDIA REPORT
SAND2015-8043
Unlimited Release
Printed September 2015

Tunable Quantum Dot Solids: Impact of Interparticle Interactions on Bulk Properties

Michael B. Sinclair, Hongyou Fan, Igal Brener, Sheng Liu, Ting S. Luk, Binsong Li

Prepared by
Sandia National Laboratories
Albuquerque, New Mexico 87185 and Livermore, California 94550

Sandia National Laboratories is a multi-program laboratory managed and operated by Sandia Corporation, a wholly owned subsidiary of Lockheed Martin Corporation, for the U.S. Department of Energy's National Nuclear Security Administration under contract DE-AC04-94AL85000.

Issued by Sandia National Laboratories, operated for the United States Department of Energy by Sandia Corporation.

Available to DOE and DOE contractors from
U.S. Department of Energy
Office of Scientific and Technical Information
P.O. Box 62
Oak Ridge, TN 37831

Telephone: (865) 576-8401
Facsimile: (865) 576-5728
E-Mail: reports@osti.gov
Online ordering: http://www.osti.gov/scitech

Available to the public from
U.S. Department of Commerce
National Technical Information Service
5301 Shawnee Rd
Alexandria, VA 22312

Telephone: (800) 553-6847
Facsimile: (703) 605-6900
E-Mail: orders@ntis.gov
Online order: http://www.ntis.gov/search

SAND2015-8043
Unlimited Release
Printed September 2015

Tunable Quantum Dot Solids: Impact of Interparticle Interactions on Bulk Properties

Michael B. Sinclair, Electronic, Optical, and Nano Materials
Hongyou Fan, Advanced Materials Laboratory
Igal Brener, Applied Photonic Microsystems
Sheng Liu, Applied Photonic Microsystems
Ting S. Luk, Nanostructure Physics
Binsong Li, Advanced Materials Laboratory
Sandia National Laboratories
P.O. Box 5800
Albuquerque, New Mexico 87185-MS1411

Abstract

QD-solids comprising self-assembled semiconductor nanocrystals such as CdSe are currently under investigation for use in a wide array of applications including light emitting diodes, solar cells, field effect transistors, photodetectors, and biosensors. The goal of this LDRD project was develop a fundamental understanding of the relationship between nanoparticle interactions and the different regimes of charge and energy transport in semiconductor quantum dot (QD) solids. Interparticle spacing was tuned through the application of hydrostatic pressure in a diamond anvil cell, and the impact on interparticle interactions was probed using x-ray scattering and a variety of static and transient optical spectroscopies. During the course of this LDRD, we discovered a new, previously unknown, route to synthesize semiconductor quantum wires using high pressure sintering of self-assembled quantum dot crystals. We believe that this new, pressure driven synthesis approach holds great potential as a new tool for nanomaterials synthesis and engineering.

CONTENTS

FIGURES

NOMENCLATURE

QD	quantum dot
SAX	small angle x-ray scattering
WAX	wide angle x-ray scattering
HP-SAX	high pressure small angle x-ray scattering
HP-WAX	high pressure wide angle x-ray scattering
UV	ultraviolet
VIS	visible
CdSe	cadmium selenide
LDRD	laboratory directed research and development
DAC	diamond anvil cell
TEM	transmission electron microscopy
SEM	scanning electron microscopy
PL	photoluminescence
WZ	wurtzite
ZB	zinc blende
RS	rock salt

1. INTRODUCTION

1.1. Background

The goal of this project was to develop a fundamental understanding of the relationship between nanoparticle interactions and the different regimes of charge and energy transport in semiconductor quantum dot (QD) solids. QD-solids comprising self-assembled semiconductor nanocrystals such as CdSe are currently under investigation for use in a wide array of applications including light emitting diodes, solar cells, field effect transistors, photodetectors, biosensors, lasers, and thermoelectrics. These unique materials exist at the crossover between isolated particles and bulk materials. They retain many of the attractive features of the isolated particles such as size-tunable bandgaps, but interparticle interactions modify their behavior and cause charge and energy delocalization. At present, the relative contributions of charge and energy transport to device performance are not well understood. For example a QD-solid solar cell with an efficiency of ~5% was recently demonstrated but conflicting explanations of the underlying mechanism have been proposed: exciton migration and dissociation at the electrodes; and direct photogeneration of electron-hole pairs. Device optimization requires a quantitative fundamental understanding of the means by which interparticle interactions lead to collective bulk behavior.

At the outset of this project, the current state-of-the-art in the study of interparticle effects relied on the utilization of different capping ligands to control the interparticle separation. However, the interpretation of experimental results is clouded by the large number of other variables that change as the ligand is varied. Our approach was to use a Sandia developed mechanical compression method, in conjunction with nanoparticle self-assembly, to fabricate QD-solids with precisely controllable interparticle spacing. State-of-the-art optical probes, including ultrafast spectroscopy were then used to characterize QD-solid behavior spanning the range from widely separated nanoparticles to sintered nanoparticle superlattices — all within a single, highly ordered QD-solid sample.

This research program focused primarily on QD-solids comprising CdSe quantum dots. These solids exhibit a fascinating spectrum of physical behavior and have been the subject of numerous investigations over the past decade. Reminiscent of molecular crystals, these solids retain many of the properties of the QD building blocks such as absorption strength and band gap energy, yet interparticle interactions induce varying degrees of charge and energy delocalization which are important for device applications. They exhibit strong optical absorption and emission which can be exploited by many non-contact optical probes to obtain information regarding the local environment, degree of excitation, and state of charge of the QDs. Furthermore, electron mobilities approaching those of bulk semiconductors have been observed in close-packed QD-solids.

Two important interparticle interactions which impact the bulk behavior of QD solids have been widely investigated: exciton migration and electron tunneling. Exciton migration occurs due to dipole-dipole interactions and the hopping rate follows a $(1/R^6)$ dependence, where R is the interparticle spacing. Exciton migration and dissociation at the

surfaces/interfaces of the QD-solid has been proposed to explain the reduced emission quantum yield observed in QD-solids, and to explain the operation of QD-solid solar cells. Exciton migration also plays an important role in non-radiative Auger recombination which occurs at high excitation densities and requires multiple excitons occupying the same dot. Electron tunneling occurs when the interparticle distance is sufficiently small that the electronic wavefunctions of neighboring particles overlap. The tunneling rate increases exponentially as the spacing is decreased and for small separations the localized wavefunctions merge to form delocalized electronic "mini-bands".

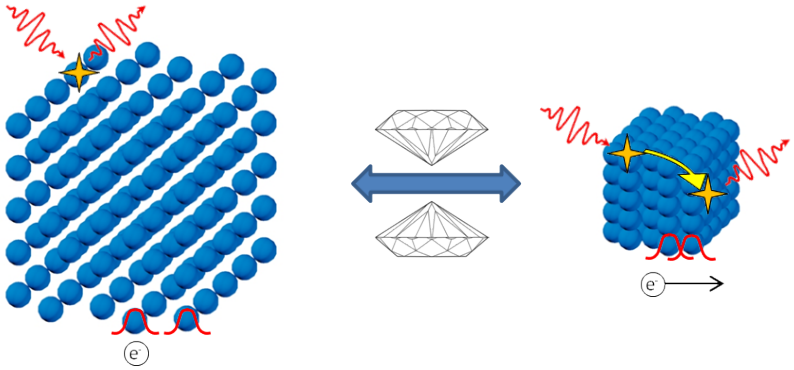

Figure 1: Pressure regulated reversible tuning of the interparticle separation in a QD-solid increases exciton mobility and allows electron tunneling as the isolated wavefunctions begin to overlap.

Tailoring the collective behavior in QD solids requires simultaneous control over two competing effects: the strength of the interparticle interactions and the degree of disorder within the solid. If one can successfully control these factors, additional interactions could be exploited to control bulk properties. For example, at very small separations the QDs can no longer be accurately represented by point dipoles, and higher-order multipoles will begin to contribute to exciton delocalization. Furthermore, exciton delocalization is expected to transition from a "hopping" regime to a coherently delocalized, quantum entangled regime reminiscent of J-bands in molecular crystals. In this case, effects such as line narrowing and superradiance might be observable. Also, phonon delocalization is expected to occur as the particles begin to touch with a concomitant modification of the electron-phonon interaction which plays an important role in Auger recombination. Furthermore, particle interactions mediated by the vibronic and electronic modes of the ligand can give rise to new charge and energy delocalization processes.

One can attempt to unravel these processes through a systematic study employing QDs with different length capping ligands. Unfortunately this approach requires that a new QD-solid sample be fabricated for each desired interparticle spacing which introduces a host of ill-controlled effects including different particle size distributions, different degrees of superlattice disorder, different tunnel barrier heights, and different electronic and vibrational mode spectra of the ligands. Each of these uncontrolled variations can have a significant effect on the outcome of a measurement, and, while general trends might be obtained, the combined effect of all of these error sources makes quantitative interpretation of results unreliable and unrepeatable for systematic understanding.

A more systematic investigation of the impact of interparticle interactions on charge and energy delocalization can be obtained through the technically more challenging strategy of pressure induced regulation of the QD-solid lattice parameter. This can be achieved by subjecting the QD-solid to hydrostatic pressure within a Diamond Anvil Cell (DAC), which allows one to continuously tune the lattice parameter over a broad range. Furthermore, the initial application of pressure within the DAC induces structural transitions and greatly reduces the defect density, resulting in highly ordered single crystals. With this approach, the complete range of particle interaction regimes can be continuously probed within a single, highly ordered QD-solid. Indeed, there have been a several studies that have employed this strategy to investigate structural properties or simple absorption/emission optical properties of colloidal semiconductor QD-superlattices.

In this research program we used mechanical compression to tune the interparticle spacing of QD-superlattices and characterize their properties using state-of-the-art structural and optical probes. We synthesized high quality monodisperse QD samples and utilized self-assembly techniques to fabricate high quality QD-superlattices. We applied hydrostatic pressure to the superlattice using a DAC equipped for optical access. Adoption of this experimental strategy necessarily requires that non-contact techniques be employed almost exclusively for the characterization of the QD-superlattice properties. Thus we relied on x-ray scattering to determine the relevant crystal structures, and advanced optical CW and transient optical spectroscopies to determine the photoexcitation dynamics.

2. QUANTUM DOT SYNTHESIS AND PRESSURE DEPENDENT PROPERTIES OF QUANTUM DOT SOLIDS

2.1. Synthesis of CdSe nanoparticles

CdSe nanoparticles were synthesized according to modified literature procedures [1]. Briefly, Se powder (14.7 mmol, 1.16 g) was dissolved in 7.22 g Trioctylphosphine (TOP) to make a 1.70 M stock solution. CdO (1.88 mmol, 0.24 g), Octadecylphosphonic acid (ODPA, 3.76 mmol, 1.26 g), Trioctylphosphonic oxide (TOPO, 31 mmol, 12 g) were loaded into a 3-neck flask, degassed and purged with Ar. The mixture was heated to 150˚C and pumped for 1 hour before it was heated to 300 ˚C under Ar. TOP (6 g) was injected into the flask and the mixture was heated to 355 ˚C. 1.72 mL Se/TOP stock solution was injected into the flask quickly. The heating mantle was removed after 20s – 180 s, depending on the desired nanoparticle size. In case of 5nm CdSe obtained here, a 1 minute reaction time was used. The reaction mixture was cooled to room temperature, and then ethanol was added to precipitate the CdSe nanoparticles. The mixture was centrifuged at 4000 rpm to obtain a crude product, which was dissolved in small amount of toluene and precipitated with ethanol again. The purified nanoparticles were pumped for 10 minutes to dry and were stored in glove box. The CdSe nanoparticles were re-dissolved in toluene and the solution was filtered through 0.45μm PTFE filter before use.

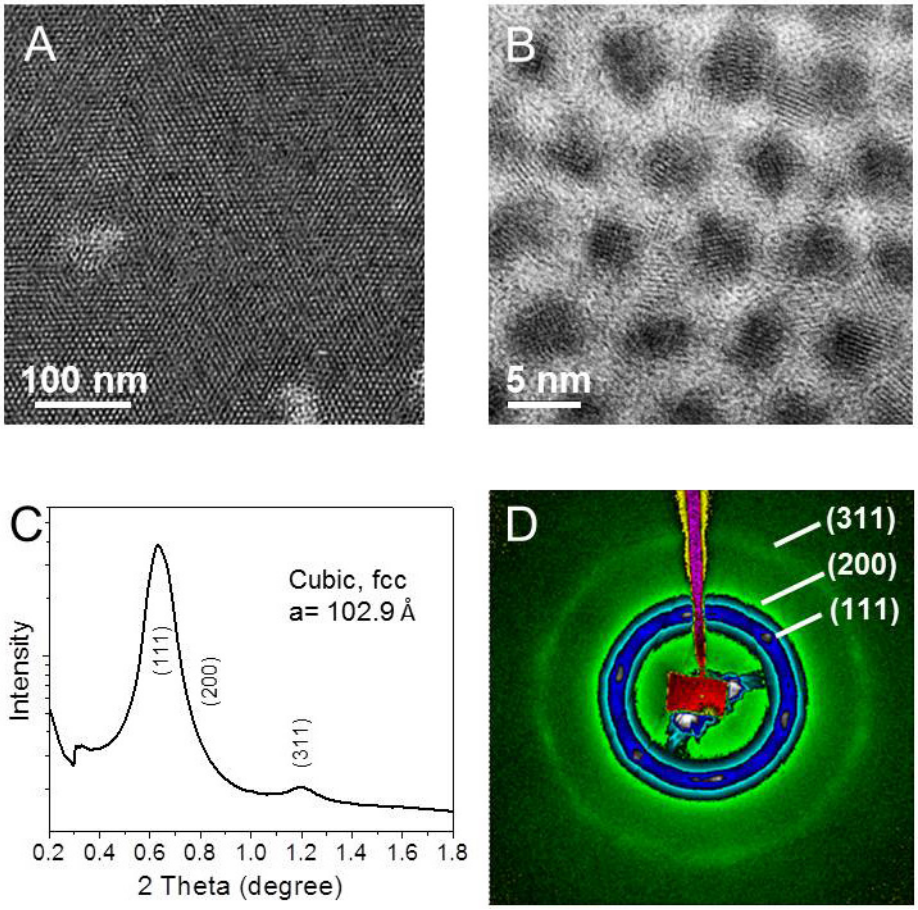

Figure 2. a) Low resolution TEM image of an ordered 5nm CdSe nanoparticle array. b) High resolution TEM image of 5 nm CdSe nanoparticles. c) Integrated SAXS spectrum of CdSe assembly from 2D SAXS image d) at 0 GPa.

The size of the CdSe nanoparticles was about 5.0 nm with a narrow distribution according to TEM images (calculated from 100 nanoparticles) (Figure 2A and 2B). The SAXS image and integrated pattern (Figure 2C and 2D) collected at ambient pressure indicate a superlattice structure specific to a face centered-cubic (fcc) mesophase with space group Fm-3m. The unit cell parameter a is calculated to be 102.9 Å.

2.2. Preparation of CdSe nanoparticle films

CdSe Nanoparticle arrays were fabricated through a solvent evaporation method by drop-casting CdSe nanoparticle solutions (100 mg/mL in toluene with 25% polystyrene) on a silicon wafer. A piece of the CdSe nanoparticle film was peeled off the silicon wafer using a needle and loaded into the diamond anvil cell (DAC) for in-situ HP-SAXS, HP-WAXS and absorption measurements

2.3. Characterization

TEM studies were performed on a JEOL 2010 with a 200-kV acceleration voltage, equipped with a Gatan slow scan charge-coupled device camera. The STEM images were obtained by an aberration-corrected scanning transmission electron microscope (AC-STEM, FEI Titan G2 8200). SEM images were taken using a Hitachi S-5200 FEG microscope at 5 kV. Ultraviolet–visible spectra were obtained on a Perkin Elmer Lambda 950 spectrophotometer. In-situ HP-SAXS and HP-WAXS measurements were performed on the B1 station at the Cornell High Energy Synchrotron Source (CHESS) with a monochromatic X-ray radiation of wavelength 0.485946Å. The distance between the sample and a large area MAR345 detector was 1341.00 mm, as determined using both CeO_2 and silver behenate powder standard. Several small ruby chips were loaded into the DAC chamber as inside pressure probes to monitor the sample pressure by a standard pressure-dependent ruby fluorescence technique. Scattering images were calibrated and integrated using the Fit2D software. The scattering curves were fitted in Gaussian distribution using the Origin 8 program. The in-situ ultraviolet–visible spectra of the ordered CdSe nanoparticle superlattice thin films during high-pressure compression and release were measured by a PerkinElmer Lambda 950 ultraviolet–visible spectrometer. The DAC loaded with CdSe nanoparticle film was inserted into the sample beam line, and a blank gasket with a 250-mm hole was inserted into the reference beam line. All other procedures were the same as regular procedures. The photoluminescence (PL) spectra of the ordered CdSe nanoparticle superlattice thin films during high-pressure compression and release were measured by a home-made fluorometer. The excitation wavelength of the PL spectra is 405 nm.

2.4. Structural evolution of CdSe nanoparticle arrays during compression

To determine the superstructure changes, in-situ HP-SAXS and HP-WAXS measurements were performed at the B1 beamline at Cornell High Energy Synchrotron Source (CHESS). Figure 3 shows the structural evolution of CdSe nanoparticle arrays during pressure-induced assembly and sintering processes.

At ambient pressure, the CdSe nanoparticle superlattice structure is face center cubic (fcc) mesophase with space group Fm-3m. The unit cell parameter, *a,* is calculated to be 102.9 Å. Upon increasing the pressure from ambient to 8 GPa, both the HP-SAXS and HP-WAXS peaks gradually shift to higher 2 theta (or lower d-spacing) (Fig. 3A, 3B), which suggests a pressure-induced shrinkage of the nanoparticle superlattice as well as the atomic lattice. The changes of *d* spacing of superlattices are fully reversible when pressure was released before the threshold pressure (~9 GPa). The superlattice structure changed from cubic to quasi hexgonal mesophase at pressure between 9.5 and 11.6 GPa, indicating the sintering of CdSe nanoparticles to bundles of CdSe nanowires with quasi hexagonal mesostructures, which is consistent with the TEM results.

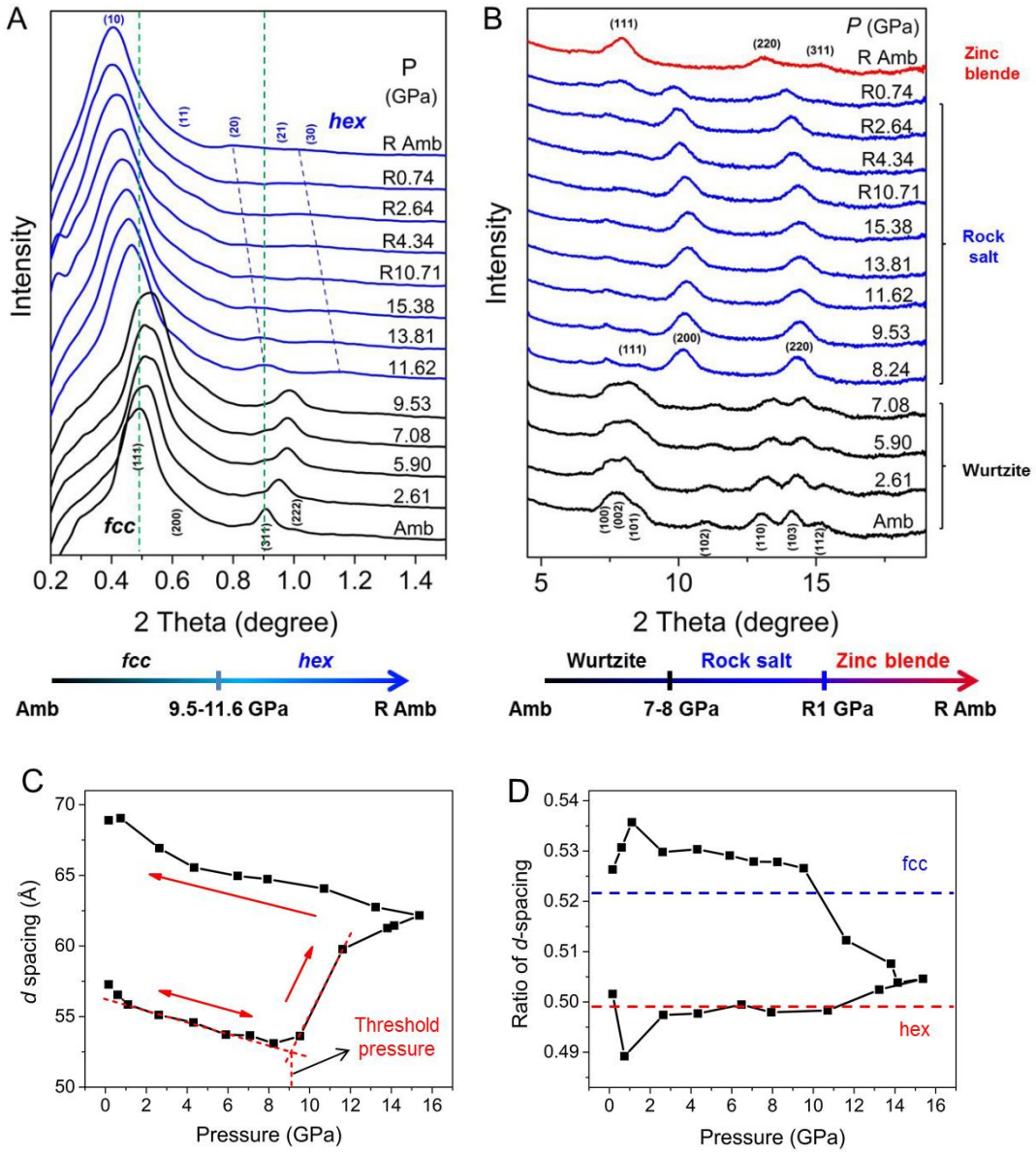

Figure 3. The integrated spectra from the (A) HP-SAXS and (B) HP-WAXS images of an ordered 5nm CdSe nanoparticle array at varied pressure. (C) The d-spacing changes of

the first Bragg reflection along with the pressure in each HP-SAXS spectrum in (A). (D) d-spacing ratio R at different pressures.

The d-spacing ratio, *R*, at varied pressure (Fig. 3D) remains almost constant below 9.5 GPa, and close to the theoretical value *R* (for example, the ratio of d-spacing of the second to the first major peak) d311/d111=0.522 for an fcc superlattice. Above 9.5 GPa, the superlattice changed obviously, and cannot be indexed to either a fcc or hexagonal mesophase. From 9.5 GPa to about 15 GPa and then releasing to around 10 GPa, *R* varied between 0.522 and 0.5. After the pressure was released to about 10 GPa, the HP-SAXS patterns were consistent with a 2D hexagonal mesophase, in which *R* (d20/d10) becomes ~0.5, which is both equal to the theoretical ratio d20/d10 for a 2D hexagonal mesophase, and consistent with the HP-SAXS indexing and TEM results.

The atomic lattice structure changed from wurtzite (WZ) to rock salt (RS) at around 7-8 GPa, then remained same until it changed to zinc blende (ZB). Small amount of wurtzite structure could be still found by TEM when the pressure was released lower than 1 GPa. The WZ to RS transformation happened at 7-8GPa, while the fcc-hexgonal superlattice transformation happened at 9.5-11.6GPa, indicating the sintering happened in RS-type CdSe NPs.

3. IN-SITU OPTICAL CHARACTERIZATON

3.1. Absorption and photoluminescence spectroscopy under pressure

In-situ UV-VIS and PL spectra were studied and the results are shown in Figure 4 during the compression from 0 - ~15 GPa. The absorption peak of the ordered CdSe nanoparticle array blue shifts from 578 nm at 0 GPa to 535 nm at 5.82 GPa due to nanoparticle aggregation under pressure. The absorption peak starts to extend to long wavelength at around 7 GPa, indicating the onset of nanoparticles sintering (to nanowires). Both the absorbance and PL are fully reversible if the pressure is kept lower than about 7 GPa (Figure 5). Upon increasing the pressure above 7 GPa, the absorption peak became weaker, because the atomic crystal structure of CdSe nanoparticles changes from wurtzite to rock salt when pressure is higher than about 7 GPa (see in-situ WAXS spectra). Absorption peak after full pressure releasing from around 15 GPa shows 10 nm red shift (from 594 nm to 604 nm) comparing to that of the starting material, indicating new nanostructures with extended length (nanowires) form.

The PL peak blue shifted from 595 nm at 0 GPa to 555 nm at 5.62 GPa while increasing pressure due to aggregation of nanoparticles. The PL peak became very weak at about 6.40 GPa. This is because the atomic lattice of CdSe nanoparticles started to change from wurtzite (direct bandgap) to rock salt (indirect bandgap) at around this pressure. Transitions across indirect band gaps are less efficient, thus CdSe in rock salt phase has weak PL [2]. The PL peak was recovered when released to ambient pressure, because the atomic lattice was changed from rock salt to zinc blende (see in-situ WAXS spectra in Figure 3). The later phase has direct bandgap, thus has stronger PL. The PL peak of the product after high pressure red shifted 9 nm and became broader, indicating formation of nanostructured CdSe such as nanorods, nanowires etc. The PL intensity of the product after pressure was released to 0GPa is about 3% of that before compression.

To further understand the relation between pressure and optical properties, the evolution of the PL spectra and UV-VIS spectra with increasing pressure are plotted in Figure 6. In this case, we used a continuous-wave, λ=405 nm diode laser as the pump for the PL spectra measurement. A λ=484 nm long pass filter was used to isolate the PL from the pump. The PL emission is generated from the electron relaxation from the conduction band minimum energy to the valence band at the point of Brillouin zone. The absorption spectra were measured using an UV-visible spectrometer (Perkin Elmer Lambda 950 UV/Vis/NIR Spectrometer) for comparison. At pressures below 6 GPa, we observe that the PL emission and absorption peak energy shifts to higher values in a near-linear fashion with increasing pressure. This indicates a transition of larger direct bandgap caused by the reduction of the QD volume at higher pressure [3]. The pressure coefficient for the direct bandgap of CdSe QDs was determined to be ~45±2 meV/GPa from the PL spectra and 49~±3 meV/GPa extracted from the absorption spectra, showing good agreement, using a quadratic fit (Figure 6). This value agrees well with previously reported value of 37 meV/GPa [4] and 58 meV/GPa [5] or 43.1 meV/GPa [3] for bulk CdSe. Above 6 GPa, we observed an abrupt decrease of the PL intensity as well as the disappearance of the sharp absorption edge due to the phase transition from direct bandgap wurtzite to indirect bandgap rock salt [6]. We also found that the PL peak wavelength mostly recovers if we release the pressure before reaching ~7 GPa (Figure 5B). However, the QDs showed significant hysteresis upon release if the pressure was applied above 7 GPa, with the rock salt structure persisting down to

below 1 GPa. A wurtzite-zinc blende structure was recovered when released to atmospheric pressure. We also observed much weaker PL intensity when the pressure is released approaching 0 GPa [7].

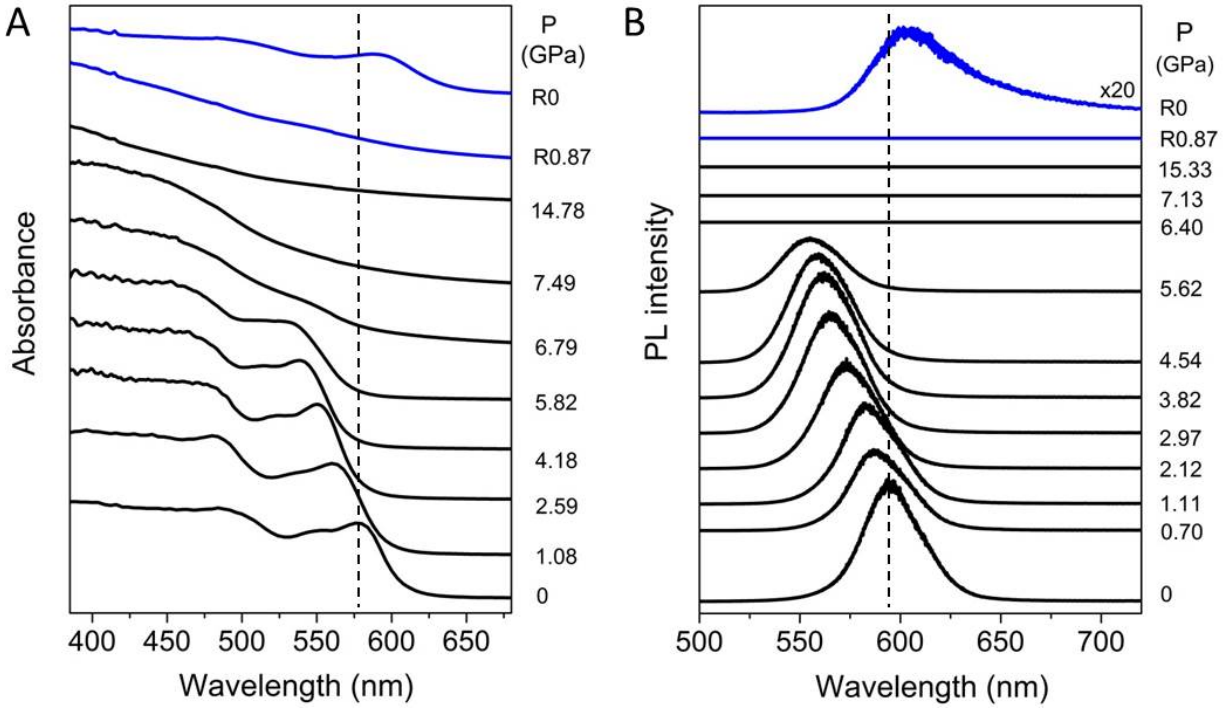

Figure 4. The in-situ (A) ultraviolet–visible spectra and (B) PL spectra of the ordered CdSe nanoparticles superlattice thin film during high-pressure compression and release.

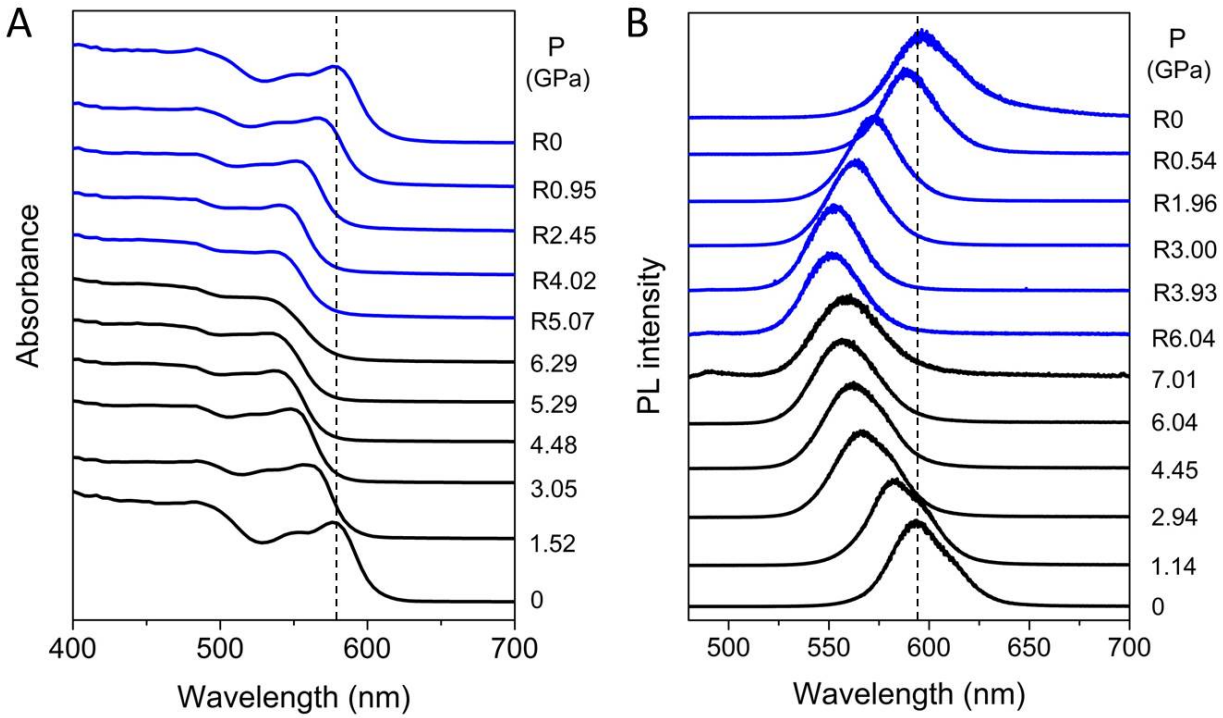

Figure 5. The in-situ (A) ultraviolet–visible spectra and (B) PL spectra of the ordered CdSe nanoparticles superlattice thin film during low-pressure compression and release.

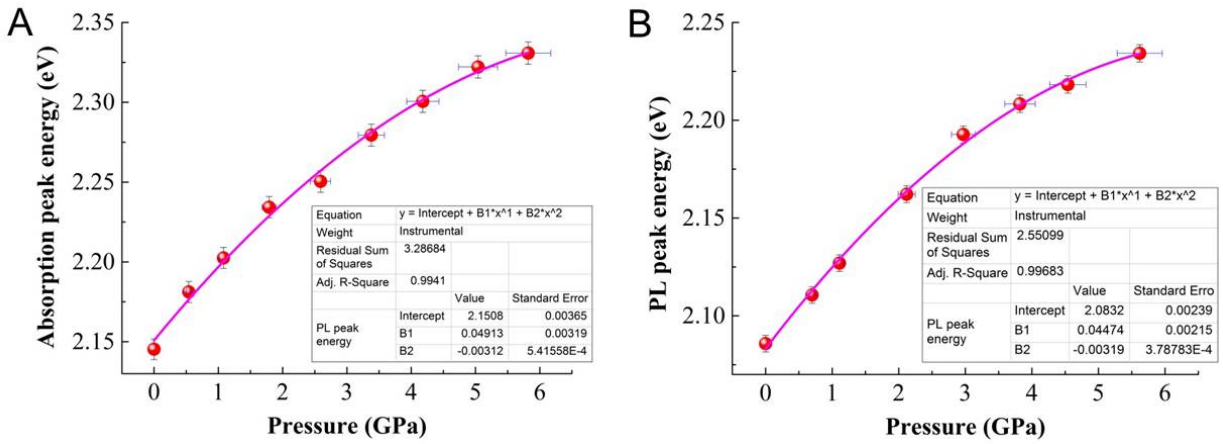

Figure 6. (A) The absorption and (B) PL emission peak energy of the ordered CdSe nanoparticles superlattice thin film at various pressure during high-pressure compression.

4. MECHANICAL PROPERTIES

4.1. Extraction of the effective bulk modulus

We used the Vinet equation (Eq. 1) and the third-order Birch-Murnaghan (B-M) equation of states (Eq. 2) to extract the effective bulk moduli for CdSe nanoparticles. In the equations, B_0 is the ambient pressure bulk modulus, B_0'- the pressure derivative of the bulk modulus (B_0'= dB_0/dP), V - the unit cell volume under pressure, and V_0 - the initial unit cell volume at ambient pressure.

$$P = 3B_0\left(\frac{V}{V_0}\right)^{-2/3}\left[1-\left(\frac{V}{V_0}\right)^{1/3}\right]\exp\{1.5(B_0'-1)\left[1-\left(\frac{V}{V_0}\right)^{1/3}\right]\} \quad (1)$$

$$P = \frac{3}{2}B_0\left[\left(\frac{V_0}{V}\right)^{7/3}-\left(\frac{V_0}{V}\right)^{5/3}\right]\{1+\frac{3}{4}(B_0'-4)\left[\left(\frac{V_0}{V}\right)^{2/3}-1\right]\} \quad (2)$$

Based on the experimental compression curves (unit cell volume vs. pressure, Figure 7), the fitted bulk modulus of CdSe is 12.3 GPa from the Vinet equation of state (Eq. 1), and 11.5 GPa from the third order B-M equation of state (Eq. 2). The bulk moduli are comparable to the threshold pressure of about 9 GPa we observed for compression of CdSe nanoparticles.

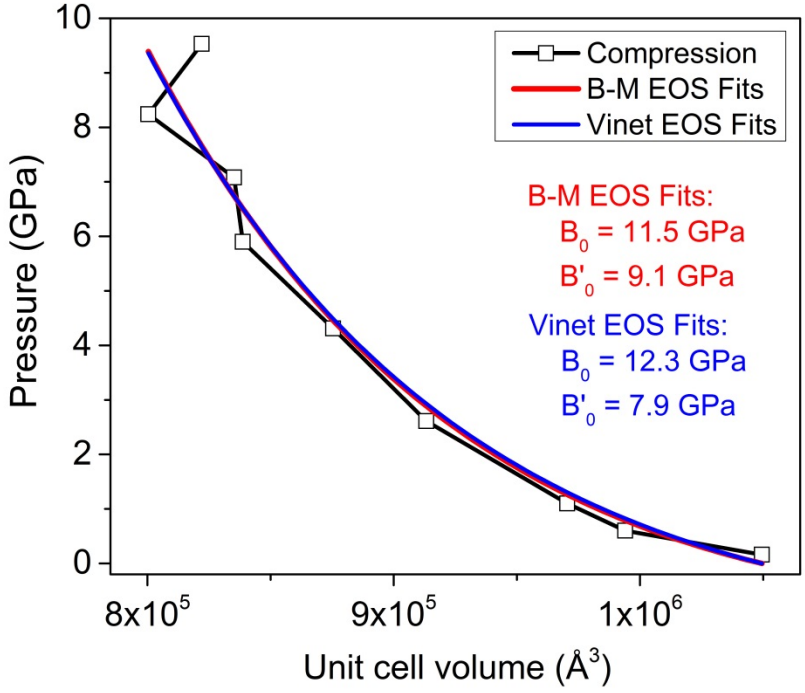

Figure 7. Experimental compression curve for CdSe (pressure as a function of unit cell volume) and the calculated bulk modulus from fitting of Birch-Murnaghan and Vinet's equation of state.

6. INVESTIGATION OF QUANTUM DOT—QUANTUM DOT COUPLING AT HIGH HYDROSTATIC PRESSURE

6.1. Introduction

Semiconductor quantum dots (QDs) have been widely used in optics and photonics applications due to their high quantum efficiency and the ability to tune the bandgap energy using quantum confinement through size control. Although the linear and nonlinear carrier dynamics of QDs have been extensively studied which provides useful information for improving material quality, less work has been done to study the inter-QD coupling. Here, we present a mechanism for tuning the inter-QD spacing by applying hydrostatic pressure. At high pressure we observe: a bandgap energy shift; a structural transition from direct bandgap wurtzite to indirect bandgap rock salt; and a radiative decay lifetime time evolution that can be attributed to QD-QD coupling.

6.2. PL spectra of CdSe QDs at high hydrostatic pressures

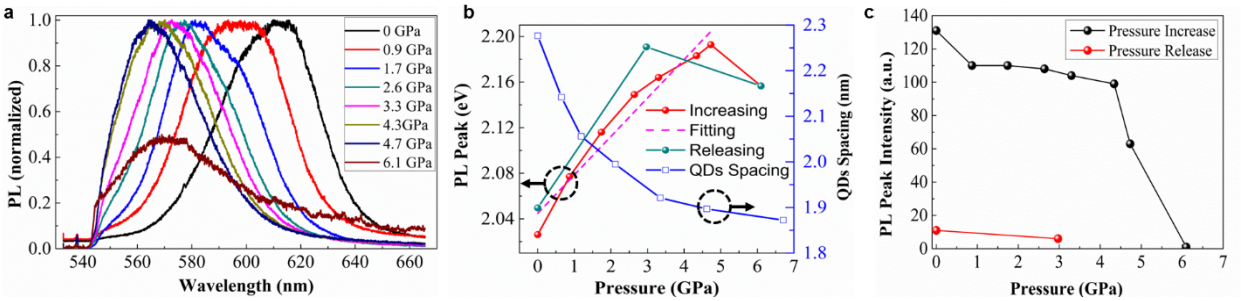

Figure 8. a) PL spectra of CdSe QDs under different hydrostatic pressures. PL peak energy (b) and intensity (c) at different pressures.

We synthesized CdSe QDs using a chemical method with n-Octadecylphosphonic acid (ODPA)/Trioctylphosphine oxide (TOPO)/Trioctylphosphine (TOP) as ligands. The QDs were nearly monodisperse with diameters of ~5 nm. The hydrostatic pressure was generated by a diamond-anvil-cell (DAC) using Silicone oil as the pressure-transmitting medium. The pressure was monitored by the spectral shift of the ruby R_1 line.

The evolution of the PL spectra with increasing pressure is shown in Fig. 8a. We used a continuous-wave, λ=532 nm laser as the pump for the PL spectra measurement. The spectral stop band at λ~536 nm is caused by a λ=536 nm long pass filter used to isolate the PL from the pump. The spectra at pressures between 0-5 GPa were normalized to the same amplitude for better comparison. At the pressure of 6.1 GPa, we normalized the PL spectrum to 0.5 instead to 1 because of the much lower PL intensity which is caused by the phase transition explained below.

At pressures below 5-6 GPa, we observe that the PL emission energy shifts to higher values in a near-linear fashion with increasing pressure. This indicates a transition of larger Γ direct bandgap caused by the reduction of the QD volume at higher pressure [3] (Fig. 8b). The pressure coefficient for the direct bandgap of CdSe QDs was determined to be ~33.7meV/GPa [8] by a linear fit of the pressure dependence of the PL spectra energy (dash line in Fig. 8b). In contrast to the blue shift at lower pressures, we observe the PL peak wavelength

to red shift at pressures greater than 6 GPa. This is caused by a structure transition from direct bandgap wurtzite to indirect bandgap rock salt [3,6,7]. This phase change also explains the abrupt decrease of the PL intensity (Fig. 8c). We also found that the PL peak wavelength mostly recovers if we release the pressure before reaching ~7 GPa (green dots in Fig. 8b). However, the intensity of PL does not fully recover showing hysteresis upon releasing the pressure (Fig. 8c). X-ray diffraction measurements show that the inter-QD spacing decreases from 2.28 nm at 0 GPa down to 1.85 nm at ~7 GPa (blue curve in Fig. 8b). This could induce stronger inter-QD coupling since the Bohr exciton radius (~5 nm) is larger than the size of QDs.

6.3. PL lifetime of CdSe QDs at different hydrostatic pressures

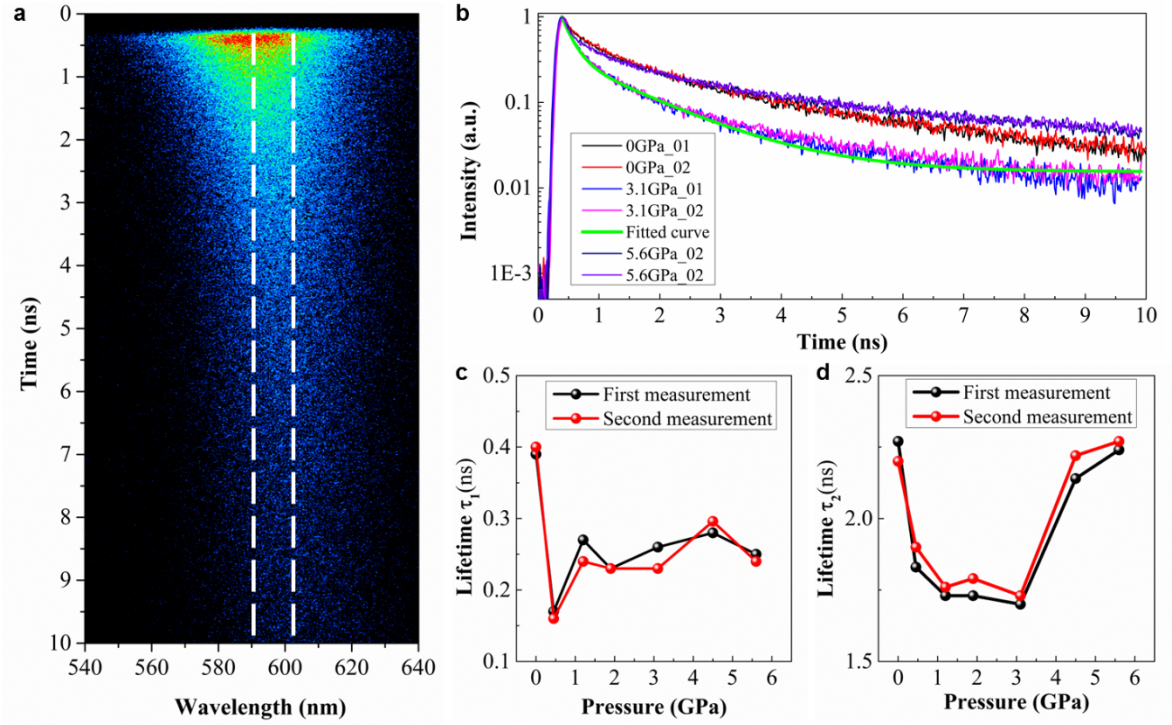

Figure 9. a) Streak camera image showing CdSe QDs PL radiation decay at 0 GPa. b) PL decay traces at selected pressures. Fitted faster (c) and slower (d) lifetimes of the PL decay traces at different hydrostatic pressures.

We used a streak camera with a grating spectrometer to measure the CdSe QDs PL decay lifetime. A frequency doubled tunable Ti:Sapphire laser was used to generate ~120 femtosecond, λ=475 nm pump pulses. A low pump power of 100 μW was used to ensure that <1 electron-hole pair was generated per CdSe QD. Fig. 9a shows a typical (specifically at 0 GPa) streak camera photon counting image containing both the spectral and temporal information. We observe a PL energy shift of ~42 meV towards lower energy at later delay time (dashed lines). Fig. 9b shows the decay traces at selected pressures extracted from 3D images similar to Fig. 9a. By fitting the data in Fig. 9b with two exponential decay constants τ_1 (shorter) and τ_2 (longer) (a fitting example at 3.1 GPa is shown as the green curve), we observe different decay lifetimes at elevated pressures as shown in Fig. 9c&d. As we apply higher pressures, the two lifetimes show different behaviors: τ_1 initially shortens to ~0.15 ns at pressure <1 GPa followed by an increase and reaches an approximately constant value at higher pressures; τ_2 continuously decreases at

pressures below 4-5 GPa down to ~1.7 ns and then recovers back to ~2.25 ns. The lifetimes' changes were likely contributed by the bandgap energy shift, the structural transition, better quantum confinement due to the shrinkage of the QDs size, and the interactions between QDs due to a smaller spacing between them.

7. CONCLUSIONS

In this project, we investigated the mechanical, structural, and optical properties of CdSe based quantum dot solids as a function of ambient pressure. Specifically, the QD-solid samples were placed in a diamond anvil cell to allow for the application of hydrostatic pressure up to ~15GPa. The structural properties were measured using both small angle, and wide angle x-ray scattering, and the optical properties were measured using a suite of CW and transient optical spectroscopies. Our results showed that at ambient pressure the QD-solid exhibits an fcc crystal structure, and the application of pressure initially reduces the inter-QD distance. As the pressure is increased further, a phase transformation to hexagonal crystal structure takes place. The hexagonal phase remains when the pressure is reduced to ambient pressure. More importantly, our wide-angle x-ray scattering shows that the CdSe crystallites themselves undergo a structural phase transition from the wurtzite structure at ambient pressure, to a rock salt structure near 6 GPa. This structural phase transition is significant since the wurtzite structure possesses a direct bandgap and, hence exhibits strong photoluminescence. In contrast, the rock salt structure possesses an indirect band gap and only exhibits weak luminescence. Ultrafast optical studies, including ultrafast photoluminescence and ultrafast photo-induced absorption reveal that the lifetime of the photo excitations decreases with increasing pressure, possibly due to phonon assisted scattering to the L-valley of the CdSe band structure. This results in non-radiative decay of the excitations and explains the dramatic decrease of photoluminescence strength. Further studies are required to more fully explain this ultrafast behavior.

4. REFERENCES

1. Z. Adam Peng and Xiaogang Peng, Formation of High-Quality CdTe, CdSe, and CdS Nanocrystals Using CdO as Precursor, *J. Am. Chem. Soc.*, vol. 123, 183-184, 2001.
2. S.H. Tolbert, A.B. Herhold, C.S. Johnson, A.P. Alivisatos, Comparison of quantum confinement effects on the electronic absorption spectra of direct and indirect gap semiconductor nanocrystals, *Phys. Rev. Lett.*, vol. 73, 3266-3269, 1994.
3. W. Shan, W. Walukiewicz, J. W. Ager Iii, K. M. Yu, J. Wu, and E. E. Haller, Pressure dependence of the fundamental band-gap energy of CdSe, *Applied Physics Letters*, vol 84, 67, 2004.
4. A. L. Edwards and H. G. Drickamer, Effect of Pressure on the Absorption Edges of Some III-V, II-VI, and I-VII Compounds, *Physical Review*, vol 122, 1149, 1961.
5. J. R. Mei and V. Lemos, *"Photoluminescence on CdSe and CdTe under hydrostatic pressure,"* Solid State Communications, vol. 52, pp. 785-788, 1984.
6. S. H. Tolbert and A. P. Alivisatos, The wurtzite to rock salt structural transformation in CdSe nanocrystals under high pressure, *Journal of Chemical Physics*, vol. 102, pp. 4642-4656, 1995.
7. S. H. Tolbert and A. P. Alivisatos, Size Dependence of a First Order Solid-Solid Phase Transition: The Wurtzite to Rock Salt Transformation in CdSe Nanocrystals, *Science*, vol. 265, pp. 373-376, 1994.
8. J. Li et al, "Optical spectra of CdSe nanocrystals under hydrostatic pressure", *J. Phys. Condens. Matter.* vol 13, 2033, 2001.

DISTRIBUTION

1	MS1411	Michael B Sinclair	1816 (electronic copy)
1	MS1411	Paul G Clem	1816 (electronic copy)
1	MS0899	Technical Library	9536 (electronic copy)
1	MS0359	D. Chavez, LDRD Office	1911 (electronic copy)


Sandia National Laboratories